Received: February 24, 2014 | Accepted: March 15, 2014 | Web Released: June 5, 2014 CL-140146

Rapid Synthesis of Cypress-like Gold Dendrites and Their Applications in Surface-enhanced Raman Scattering and Catalysis

Wenyu Tao,[1,2,3] Aiwu Zhao,*[2,3] Xucheng Chen,[1,2] Zibao Gan,[2] Qian Gao,[2] Dapeng Wang,[2] and Hongyan Guo[2]
[1]*Department of Chemistry, University of Science and Technology of China, Hefei, Anhui 230026, P. R. China*
[2]*Institute of Intelligent Machines, Chinese Academy of Sciences, Hefei, Anhui 230031, P. R. China*
[3]*State Key Laboratory of Transducer Technology, Chinese Academy of Sciences, Hefei, Anhui 230031, P. R. China*

(E-mail: awzhao@iim.ac.cn)

In this work, high-quality cypress-like Au dendrites were successfully synthesized by a fast, green, and cost-effective method. Time-dependent morphological evolution experiments revealed the growth process. The as-prepared Au dendrites with nanoscale roughness exhibited both excellent surface-enhanced Raman scattering (SERS) and high catalytic activity, indicating their potential applications in catalysis and SERS-related detection and analysis.

Au nanomaterials have attracted considerable interest in recent years owing to their potential applications in catalysis, electronics, biosensing, and surface-enhanced Raman scattering (SERS).[1–3] SERS is a powerful analytical tool, which can detect and identify analytes at very low concentrations, even down to single-molecular level.[4] Electromagnetic (EM) and chemical mechanisms are widely accepted as the two main mechanisms responsible for SERS.[5,6] The EM mechanism is closely related to surface plasmon resonance (SPR), which leads to an immense amplification of the local electromagnetic field. The chemical mechanism is due to the interaction between adsorbed molecules and metal. Usually, the EM mechanism makes the major contribution to SERS.

To date, considerable effort has been devoted to synthesize various shape-controlled Au nanostructures.[7–10] In particular, nanostructures with 3D (three-dimensional)-textured surface such as nanodendrites have drawn wide attention because of their complex morphologies containing nanoscale junctions and high surface areas. Consequently, several approaches to fabricate these dendritic structures have been explored.[11–13] Nevertheless, most of these preparative methods involve the addition of templates or surfactants, which introduce heterogeneous impurities and limit their practical application. In comparison, the galvanic replacement reaction is a more attractive route to construct dendritic nanostructures because noble metal ions could be directly reduced by an active metal.[14,15] Typically, Al foil is an ideal reducing metal owing to its reasonable price and a lower redox potential than most metal ions. However, it has been reported that the thin Al_2O_3 layer on the surface of Al foil hindered the galvanic displacement from $AgNO_3$ solution and that toxic additives such as fluorides were essential to remove the Al_2O_3 layer to promote the reaction.[16]

Interestingly, we found that the galvanic displacement between Al foil and $H[AuCl_4]$ could easily proceed without any additives such as surfactants or fluorides; therefore, the preparation of Au nanocrystals is a clean and green method. Large-scale cypress-like Au nanodendrites with high quality could be obtained by immersing the Al foil in $H[AuCl_4]$ for a specific amount of time (30 min typically), as shown in Scheme 1. For SERS detection, the Au-coated Al foil was taken out and washed carefully with ethanol. Subsequently, it was immersed in an ethanol solution of 4-aminothiophenol (4-ATP) for 3 h followed by washing with ethanol and drying in air. Raman measurements were conducted on a portable Raman spectrometer with an excitation wavelength of 785 nm. For the catalysis reaction, the Au nanodendrites were scraped from the Al foil by a powerful ultrasonic treatment in deionized water for half an hour followed by drying in a vacuum drying oven. In a representative catalysis reaction, 0.1 mL of a 0.1 M ice-cold $NaBH_4$ solution was added to 3 mL of a 1×10^{-4} M 4-nitrophenol (4-NP) solution in the presence of 0.1 mg of Au dendrites. The progress of the reaction was then monitored by recording time-dependent UV–vis absorption spectra of the mixture at 5-min intervals.

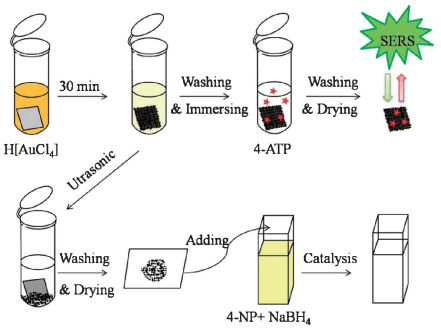

Scheme 1. Schematic illustration of the cypress-like Au dendrites.

The morphology and microstructure of the sample were examined by SEM, TEM, and HRTEM. Figures 1a and 1b show typical SEM images of the Au dendrites synthesized by a galvanic replacement reaction with 5 mM $H[AuCl_4]$ for 30 min at ambient temperature. The low-magnification SEM image (Figure 1a) reveals that a large quantity and good uniformity of Au dendrites were achieved using this approach. Figure 1b is a higher-magnification SEM image that clearly shows that the Au dendrites are composed of several aggregated nanoparticles of approximately 55-nm size. The representative TEM image of the Au dendrites is presented in Figure 1c. HRTEM was also applied for the determination of the crystal orientation of the obtained Au dendrites (Figure 1d). The clear lattice fringe with a *d* spacing of 0.236 nm confirms that the obtained Au dendrites are preferentially dominated by (111) facets. The XRD pattern recorded on the same sample is displayed in Figure S1.[17] The five diffraction peaks are assigned to the (111), (200), (220), (311), and (222) planes of the face-centered cubic Au (JCPDS 04-0784). These planes with sharp peaks indicate that the Au

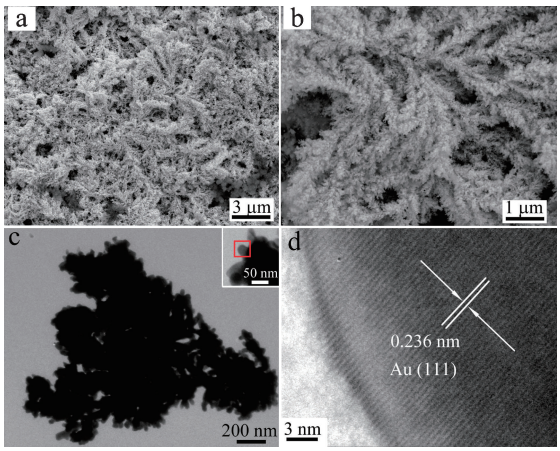

Figure 1. (a, b) SEM, (c) TEM, and (d) HRTEM images of the as-synthesized cypress-like Au dendrites. The inset is an enlarged view and the HRTEM is from the area marked with a box.

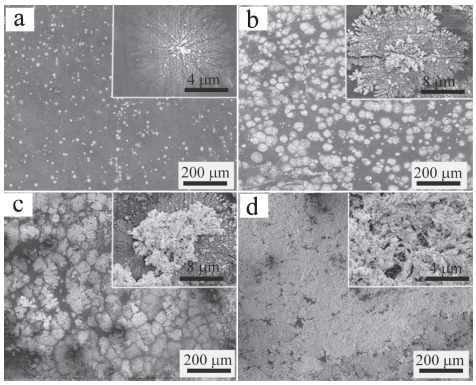

Figure 2. SEM images of dendritic Au nanostructures obtained on Al foil at different periods: (a) 10 s, (b) 2 min, (c) 10 min, and (d) 20 min. The insets are corresponding enlarged views.

dendrite particles are well crystallized. Furthermore, the EDX spectrum also confirms the high purity of the Au dendrites (Figure S2). The other elements detected in the samples originate from the copper grids.

Figure 2 shows the Au products grown on an Al substrate at early growth stages of the Au dendrites. After 10 s of reaction, some snow-like Au microflowers formed on the Al substrate (Figure 2a). When the reaction time was prolonged to 2 min, several bigger microflowers appeared and small branches grew from the center and edge of the flower (Figure 2b). Extended and well-defined Au dendrites were developed at 10 min (Figure 2c), and the underlying microflowers intercrossed each other at this time. After the Au microflowers covered the whole substrate surface, the growth of the Au dendrites dominated the growth process, and finally the Al foil was carpeted with a large area of the Au dendrites, as seen in Figure 2d. Briefly, Au atoms reduced from $H[AuCl_4]$ rapidly nucleated at random positions on the Al foil in the beginning. Later, the subsequent free Au atoms were captured to form dendrites. In a previous report, the galvanic displacement reaction between pure Al foil and an

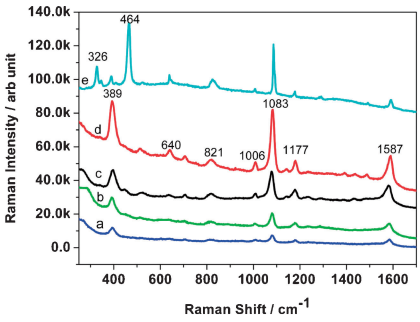

Figure 3. SERS spectra of 4-ATP adsorbed on the cypress-like Au dendrites with different concentrations (a) 10^{-9}, (b) 10^{-7}, (c) 10^{-5}, and (d) 10^{-3} M. (e) Normal Raman spectrum of 4-ATP solid powder.

$AgNO_3$ solution was hardly observed because of the existence of a thin Al_2O_3 layer on the surface of the Al foil.[15,16] It is interesting that the galvanic displacement between the Al foil and $H[AuCl_4]$ can proceed quickly. This may be due to the small amount of free Cl^- generated from the hydrolysis reaction of the $[AuCl_4]^-$ in the aqueous $H[AuCl_4]$ solution: $[AuCl_4]^- + 2H_2O \rightleftharpoons [AuCl_3(OH)]^- + [H_3O]^+ + Cl^-$.[18] Similar to F^-, the ionic radius of Cl^- is small, and the Cl^- ions have strong complexation ability to metal ions. Therefore, they can effectively dissolve the Al_2O_3 layer and induce the formation of well-defined dendritic structures.[19] The growth of the Au dendrites with different concentrations of aqueous $H[AuCl_4]$ solutions was also investigated, and the obtained Au crystals are presented in Figure S3. It is found that $H[AuCl_4]$ concentration has weak effect on the formation of the Au dendrites. When $H[AuCl_4]$ concentration is high or low, Au dendrites with a similar shape were obtained.

To evaluate the SERS performance of the prepared Au dendrites, 4-ATP was used as the probe molecule because of its enormous Raman cross section and strong adsorbability onto Au nanoparticles. Figure 3 shows the SERS spectra of 4-ATP with different concentrations ranging from 10^{-9} to 10^{-3} M (spectrum a to d) adsorbed on the as-obtained Au dendrites and the normal Raman spectrum of 4-ATP solid powder (spectrum e). As shown in spectrum d, the two strong vibrations at 1083 and 1587 cm^{-1} are assigned to a_1 vibrational modes, which are mainly from the EM field effect.[20,21] Furthermore, the enhancement of b_2 modes located at 1438 and 1492 cm^{-1} are ascribed to the charge transfer from the metal to the adsorbed molecules,[22] which demonstrates strong adsorption of 4-ATP on the Au nanostructure surfaces by the formation of a strong Au–S bond. The band at 389 cm^{-1} is assigned to one of the vibration modes of the C–S bond, most likely the bending mode of the C–S bond.[21] The estimation of SERS enhancement factors (EFs) is a criterion to judge the enhancement ability of a substrate. Here, the EF for 4-ATP on the Au substrate was calculated according to the typical equation: $EFs = (I_{SERS}N_{bulk})/(I_{bulk}N_{SERS})$,[23] where I_{SERS} and I_{bulk} are the intensities in the SERS and normal Raman spectrum, respectively. N_{SERS} and N_{bulk} are the numbers of the probe molecules illuminated by the laser spot. According to the experimental condition, the EFs for the vibrational modes at 1083 (a_1) and 1492 cm^{-1} (b_2) were 1.45×10^4 and 3.38×10^4, respectively, which are about three to four times higher than that

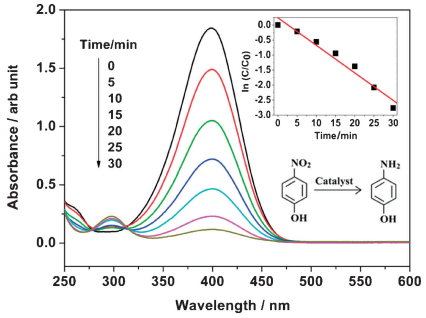

Figure 4. Successive UV–vis absorption spectra of the reduction of 4-NP catalyzed by Au dendrites. The inset is linear correlation of $\ln(C/C_0)$ versus reaction time.

on the monolayer of Au nanospheres and are comparable to that on Au nanorods.[24] The excellent SERS performances are attributed to high local fields created by nanoscale roughness. It has been widely accepted that the so-called "hotspots" such as sharp tips or small gaps of nanoparticles generate enormous local fields related to the localized SPR of Au nanoparticles.[25] The as-fabricated Au nanodendrites were composed of many tiny nanoparticles with high curvature. Moreover, the 3D-textured surfaces supplied sufficient interlaced nanojunctions. Both the tips and junctions of the Au nanoparticles made important contributions to the strong enhancement of the Raman signal.

Then, the reduction of 4-NP by $NaBH_4$ was selected as a model catalytic reaction to evaluate the catalytic activity of the Au dendrites. The original absorption peak of 1×10^{-4} M 4-NP centered at 317 nm shifted to 400 nm after the addition of a freshly prepared ice-cold $NaBH_4$ solution. The reaction was monitored by time-dependent UV–vis absorbance at 400 nm. Figure 4 shows a typical evolution process of the UV–vis spectra of 4-NP during the catalytic degradation with the Au dendrites. The peak intensity decreased and almost disappeared within 30 min after the addition of a few Au dendrites, indicating the Au dendrites indeed possessed efficient catalytic activity for the reduction of 4-NP. On account of excess $NaBH_4$ present in the solution, the reaction can be considered to follow the first-order kinetics. The rate constant (k) of this catalytic reaction is described as: $-\ln(C/C_0) = kt$, where C_0 is the initial concentration and C is the concentration after the reaction occurred for a period of time. The value of C/C_0 was measured from the relative intensity of the respective absorbance, A/A_0. On the basis of the plot of $\ln(C/C_0)$ versus time (inset in Figure 4), k was estimated to be 0.093 min^{-1}. To compare the catalytic activity of the dendrites with other nanostructures, we also calculated the activity factor k': $k' = k/m$, where m is the total weight of the catalyst. The computed results show the k' of the Au dendrites was 44 times larger than that of spongy Au nanocrystals (0.35 s^{-1} g^{-1}) reported previously.[26]

In summary, we successfully synthesized cypress-like Au dendrites by a facile and green method based on a galvanic replacement reaction. Through a series of time-dependent morphological evolution experiments, the growth process of the Au nanostructures was systematically investigated. By using 4-ATP as a probe molecule, it was found that the as-prepared Au dendrites exhibited excellent SERS performance with a detection limit of 10^{-9} M. Furthermore, the Au dendrites also displayed high catalytic activity toward the reduction of 4-NP by $NaBH_4$. It is believed that such textured Au dendrites may have potential applications in SERS, catalysis, in the construction of nanodevices, and so forth.

This work was supported by the National Natural Science Foundation of China (No. 61378038), the National Basic Research Program of China (No. 2011CB302103). We also acknowledge the support of the State Key Laboratories of Transducer Technology.

References and Notes

1 M. Haruta, M. Daté, *Appl. Catal., A* **2001**, *222*, 427.
2 X. Dong, W. Huang, P. Chen, *Nanoscale Res. Lett.* **2011**, *6*, 60.
3 C. E. Talley, J. B. Jackson, C. Oubre, N. K. Grady, C. W. Hollars, S. M. Lane, T. R. Huser, P. Nordlander, N. J. Halas, *Nano Lett.* **2005**, *5*, 1569.
4 N. P. W. Pieczonka, R. F. Aroca, *Chem. Soc. Rev.* **2008**, *37*, 946.
5 J. R. Lombardi, R. L. Birke, *J. Phys. Chem. C* **2008**, *112*, 5605.
6 X. Wang, W. Shi, G. She, L. Mu, *J. Am. Chem. Soc.* **2011**, *133*, 16518.
7 H. Ataee-Esfahani, N. Fukata, Y. Yamauchi, *Chem. Lett.* **2010**, *39*, 372.
8 T. K. Sau, A. L. Rogach, *Adv. Mater.* **2010**, *22*, 1781.
9 J. Xiao, L. Qi, *Nanoscale* **2011**, *3*, 1383.
10 D. Wang, Y. Liu, X. Zhou, J. Sun, T. You, *Chem. Lett.* **2007**, *36*, 924.
11 D. Huang, X. Bai, L. Zheng, *J. Phys. Chem. C* **2011**, *115*, 14641.
12 J. Zhang, L. Meng, D. Zhao, Z. Fei, Q. Lu, P. J. Dyson, *Langmuir* **2008**, *24*, 2699.
13 T. Huang, F. Meng, L. Qi, *Langmuir* **2010**, *26*, 7582.
14 L. Su, W. Jia, D. P. Manuzzi, L. Zhang, X. Li, Z. Gu, Y. Lei, *RSC Adv.* **2012**, *2*, 1439.
15 A. Gutés, C. Carraro, R. Maboudian, *J. Am. Chem. Soc.* **2010**, *132*, 1476.
16 W. Ye, Y. Chen, F. Zhou, C. Wang, Y. Li, *J. Mater. Chem.* **2012**, *22*, 18327.
17 Supporting Information is available electronically on the CSJ-Journal Web site, http://www.csj.jp/journals/chem-lett/index.html.
18 F. A. Cotton, G. Wilkinson, C. A. Murillo, M. Bochmann, *Advanced Inorganic Chemistry*, 6th ed., John Wiley & Sons, New York, **1999**.
19 J. Fu, W. Ye, C. Wang, *Mater. Chem. Phys.* **2013**, *141*, 107.
20 Y. Wang, H. Chen, S. Dong, E. Wang, *J. Chem. Phys.* **2006**, *125*, 044710.
21 M. Osawa, N. Matsuda, K. Yoshii, I. Uchida, *J. Phys. Chem.* **1994**, *98*, 12702.
22 Q. Zhou, X. Li, Q. Fan, X. Zhang, J. Zheng, *Angew. Chem., Int. Ed.* **2006**, *45*, 3970.
23 X. Bai, Y. Gao, H.-g. Liu, L. Zheng, *J. Phys. Chem. C* **2009**, *113*, 17730.
24 X. Hu, T. Wang, L. Wang, S. Dong, *J. Phys. Chem. C* **2007**, *111*, 6962.
25 T. Jensen, L. Kelly, A. Lazarides, G. C. Schatz, *J. Cluster Sci.* **1999**, *10*, 295.
26 M. H. Rashid, R. R. Bhattacharjee, A. Kotal, T. K. Mandal, *Langmuir* **2006**, *22*, 7141.

